IEEE Access
Multidisciplinary ⋮ Rapid Review ⋮ Open Access Journal

Received 20 September 2023, accepted 7 October 2023, date of publication 11 October 2023, date of current version 17 October 2023.

Digital Object Identifier 10.1109/ACCESS.2023.3323896

RESEARCH ARTICLE

Adaptive Control of a Constrained First Order Sliding Mode for Visual Formation Convergence Applications

JISHNU KESHAVAN, (Member, IEEE), SAURABH BELGAONKAR, AND SHREERAM MURALI
Department of Mechanical Engineering, Indian Institute of Science, Bengaluru, Karnataka 560012, India

Corresponding author: Jishnu Keshavan (kjishnu@iisc.ac.in)

This work was supported in part by the Institute of Eminence under Grant IE/RERE-21-0537.08, and in part by the Science and Engineering Research Board (SERB) Core Research Grant.

ABSTRACT Most existing solutions that guarantee finite-time convergence of a constrained first-order sliding mode either assume that the structure of the perturbation is known *apriori*, or the perturbation and its derivative are bounded by unknown constants. Moreover, convergence is usually guaranteed only in a small domain of attraction of the predefined constrained region through discontinuous control action. In contrast with these approaches, the sliding mode is assumed to be subject to perturbations with a state-dependent structure in this study, and two adaptive integral control strategies are proposed that guarantee finite-time convergence of this perturbed sliding mode from any initial condition within the predefined constrained region. First, an invertible nonlinear map is used to transform the constrained system into a constraint-free system, and an adaptive integral control strategy is used to guarantee finite-time convergence of the resulting sliding mode to a uniform ultimate bound using continuous and bounded control action. Subsequently, an alternative barrier-function based adaptive control policy is synthesized that ensures sliding mode convergence in a prescribed time to a prescribed bound that is independent of the magnitude of the perturbation term. Experimental studies of vision-based leader-follower formation control are used to validate and demonstrate superior performance of the proposed schemes compared to leading alternative designs.

INDEX TERMS Sliding mode, adaptive control, finite-time convergence, state constraint, state-dependent uncertainty.

I. INTRODUCTION

The problem of finite-time convergence of a perturbed first-order sliding mode (FOSM) when subjected to a state constraint is considered in this study. This is a problem of fundamental importance with direct relevance to robotic applications such as visual formation tracking and visual servo control, where the camera's field-of-view constraints need to be explicitly taken into account for successful realization of the tracking objective [1].

Conventional sliding mode algorithms tackle this problem by relying on prior knowledge of the upper bound of the perturbation term to synthesize discontinuous control action that guarantees finite-time convergence. This leads to overestimation of the control gains resulting in high-frequency chatter, which is a major drawback during practical implementation [2]. While chattering effects can be mitigated by switching to saturation function-based control that guarantees convergence to a boundary layer, the lack of prior information of the disturbance's upper bound motivates the need for adaptive sliding mode control (ASMC) strategies where control gains are designed to adapt to the disturbance online [3].

Adaptive first-order sliding mode control (FOSMC) strategies can be broadly classified under three categories based on the adaptation of control gains: monotonically

The associate editor coordinating the review of this manuscript and approving it for publication was Min Wang.

increasing FOSMC [4], [5], equivalent control FOSMC [6], [7], and increasing-decreasing FOSMC that assume that the perturbation and/or its derivative are bounded by unknown constants [8], [9], [10], [11], [12], [13], [14], [15], or that the perturbation satisfies a fairly restrictive growth condition that is known *apriori* [16], [17], [18], [19], or rely on discontinuous control action to achieve convergence [10], [12]. Unconventional fuzzy logic controllers have also been developed in [20] and [21] under the assumption that the state-dependent approximation error is bounded by an unknown constant. Adaptive control strategies have also been developed for a class of nonlinear systems that guarantee prescribed performance for systems with unknown control direction [22], as well as those that rely on monitoring and barrier functions to achieve prescribed-bound convergence in a fixed- or prescribed-time [23], [24]. Moreover, an additional complication arises by relying on homogeneity assumptions that no longer hold true in the presence of state constraints, which renders some of these schemes inapplicable [25].

Recent ASMC strategies using barrier functions for achieving predefined time convergence to a prescribed bound have also been considered in [11] and [12], where the size of the ultimate bound is independent of the disturbance magnitude. However, these studies suffer from a lack of global stability guarantee, causing the system to break down if the system trajectory escapes from the prescribed bound in the event of a sudden change in the switching gain which limits its practical applicability. In a recent study [13], these drawbacks are sought to be overcome by relying on the time-based generator system to adaptively tune control gains online so as to ensure prescribed-time prescribed bound (PTPB) convergence through continuous and bounded control action even in the face of a sudden change in the magnitude of the exogenous disturbance. However, this study does not account for state constraints as well as the state-dependent structure of the perturbation term, thus possibly leading to large tracking errors and limiting its applicability to practical systems [3].

The problem of controller synthesis for constrained nonlinear systems has also been considered in [26], [27], [28], and [29]. In particular, the studies in [26] and [27] consider the synthesis of a second-order sliding mode for a constrained and perturbed double-integrator system, where the control policy is shown to drive the system states to zero in a finite-time along with guaranteed satisfaction of state constraints. In contrast, the study in [28] considers the problem of controller synthesis for nonlinear systems subject to input and state constraints that ensures maximization of the attendant domain of attraction. However, a common drawback of these studies is that they only guarantee finite-time convergence in a small domain of attraction of the predefined region, whereas the objective of the current study is the synthesis of an adaptive control policy that guarantees finite-time convergence from any initial condition located within the *predefined* state constraint set. Finally, the study in [29] realizes a discontinuous control policy for state-constrained higher-order systems with perturbation having a known upper bound, where the policy is used to ensure that constraint violation does not last beyond a finite-time which may be adjusted through controller parameter tuning. Thus, in essence, the approaches proposed in [26], [27], [28], and [29] cannot be applied to the system considered in this study. To the best of this author's knowledge, the problem of synthesizing a continuous control policy for state-constrained FOSM subject to an exogenous disturbance (with an unknown upper bound) is still an area of open research.

In order to overcome these drawbacks, two novel adaptive strategies are considered in this study. First, an invertible nonlinear mapping is invoked to transform the constrained system into a constraint-free system that is perturbed by a state-dependent uncertainty term. Then, inspired by recent results in ASMC literarture [3], [30], a proportional-integral (PI) sliding mode is constructed and a state-dependent control policy is synthesized that guarantees finite-time convergence of the unconstrained error to a uniform ultimate bound (UUB) using continuous (and bounded) control action. Then, an alternative ASMC scheme is also synthesized in this study that offers the advantage of realizing continuous control action to accomplish prescribed-time convergence to a prescribed bound that is independent of the size of the perturbation term. It is shown that this approach is the key to ensuring finite-time convergence of the constrained system to a small bound with attendant satisfaction of state constraints. The following are the key contributions of this study:

- This study guarantees uniform finite-time FOSM convergence through the synthesis of ASMC schemes that realize continuous and bounded control action in the face of (possibly) stringent state constraints and unknown exogenous perturbations.
- In contrast with standard ASMC approaches that invoke *apriori* boundedness of the system state in order to guarantee finite-time convergence, the proposed state-dependent ASMC strategies are synthesized with state boundedness shown *aposteriori* and finite-time convergence achieved from any initial condition located within the predefined stateconstraint set.
- The proposed schemes are shown to provide a systematic pathway to accomplish robust tracking control though adaptive regulation of a PI sliding mode.

Moreover, in contrast with the schemes proposed in this study, note that standard ASMC schemes such as [3], [12], and [13] cannot be easily integrated in PI control loops due to a lack of integral action. Experimental studies for achieving accurate ground robot formation control using visual feedback are further used to validate the proposed schemes. A performance comparison study with the leading alternative ASMC schemes in [1], [12], [13], and [31] is also used to illustrate the advantages and superior performance of the proposed schemes.

The rest of this article is organized as follows. In Section II, the mathematical framework describing the constrained and perturbed FOSM dynamical system is formulated, which is

used in Section III to present the design of a robust ASMC policy that relies on a nonlinear state transformation and leverages state-dependent structure of the resulting perturbation term to accomplish finite-time convergence. Section IV presents an improved scheme that guarantees convergence of the FOSM to a user-prescribed bound in prescribed finite-time. In Section V, experimental demonstration of mobile robot-based visual formation control is used to provide further validation of the proposed schemes. A performance comparison study with a leading alternative ASMC design is also undertaken to demonstrate the advantages of the proposed schemes. Section VI presents the conclusions of this study.

Throughout the rest of this article, the following notations will be used. For a given vector $\boldsymbol{x} = [x_1, \ldots, x_n]^\top \in \mathbb{R}^n$, and for a real number $r \in \mathbb{R}$, the multivariable sign function is defined as $\lceil \boldsymbol{x} \rfloor^0 = \boldsymbol{x}/||\boldsymbol{x}||$, and $\lceil \boldsymbol{x} \rfloor^r = ||\boldsymbol{x}||^r \lceil \boldsymbol{x} \rfloor^0$. For a function $\boldsymbol{f}(t) \in \mathbb{R}^n \forall n \in [1, \infty)$, $\boldsymbol{f}(t) \in \mathcal{L}_\infty$ when $\sup_t ||\boldsymbol{f}(t)|| < \infty$, where $||.||$ denotes the 2-norm in $\mathbb{R}^n$. Finally, $\lambda_{\min}\{\boldsymbol{P}\}$ and $\lambda_{\max}\{\boldsymbol{P}\}$ denote the minimum and maximum eigenvalues of the symmetric positive definite matrix $\boldsymbol{P}$.

II. PROBLEM STATEMENT

Consider the following perturbed first-order system

$$\dot{\boldsymbol{x}}(t) = \boldsymbol{\alpha}(\boldsymbol{x}, t) + \beta(\boldsymbol{x}, t)\boldsymbol{\Phi}\boldsymbol{u}(t) \tag{1}$$

where $\boldsymbol{x}(t) \in \mathbb{R}^n$ is the state vector that is assumed available for feedback, $\boldsymbol{\Phi}$ is a known invertible regressor coefficient, $\boldsymbol{u}(t) \in \mathbb{R}^n$ is the control input, and $\boldsymbol{\alpha}(\boldsymbol{x}, t) \in \mathbb{R}^n$ is a state-dependent external disturbance. The parameter $\beta(\boldsymbol{x}, t)$ is an uncertain positive function such that $\overline{\beta} \geq \beta(\boldsymbol{x}, t) \geq \underline{\beta} > 0$, where $\overline{\beta}$ exists but is unknown, and $\underline{\beta}$ is a known constant [11], [12], [25].

Assumption 1: The perturbation $\boldsymbol{\alpha}(\boldsymbol{x}, t)$ is a uniformly bounded function with an upper bound that can be decomposed as $||\boldsymbol{\alpha}(\boldsymbol{x}, t)|| \leq \max\{\alpha_0(\boldsymbol{x}), 1\}\overline{\alpha}$, where $\alpha_0 : \mathbb{R}^n \to \mathbb{R}_{>0}$ is a known (and possibly nonlinear) function, and the bound $\overline{\alpha} > 0$ exists but is unknown.

Remark 1: Assumption 1 is motivated by practical considerations that is naturally satisfied by a large class of Euler-Lagrangian systems [3], and is a common assumption invoked in standard ASMC literature [3], [25], [31]. Furthermore, the structure of the upper bound of this perturbation term in Assumption 1 is more general compared to the studies in [12] and [13] that assume a constant upper bound *apriori*, and the studies in [16], [17], [18], [19], [20], and [21] which assume the upper bound to satisfy a restrictive growth condition in order to accomplish convergence. Finally, the assumption that the regressor coefficient $\boldsymbol{\Phi}$ is invertible ensures that the relative degree of the sliding variable $\boldsymbol{\sigma}$ (to be defined below) with respect to the control input $\boldsymbol{u}$ is one, which is similar to the assumption invoked in [8], [9], [10], [11], [12], and [13].

The objective of current study is to synthesize an adaptive multivariable control policy $\boldsymbol{u}(t)$ that drives the state $\boldsymbol{x}(t)$ to a small bound around the origin in finite-time under the constraint $\boldsymbol{x}(t) \in [\boldsymbol{\delta}_1, \boldsymbol{\delta}_2]$, with $\boldsymbol{\delta}_1, \boldsymbol{\delta}_2 \in \mathbb{R}^n$ being known constants satisfying $\boldsymbol{\delta}_2 > \boldsymbol{0} > \boldsymbol{\delta}_1$. Note that the state constraint condition violates the homogeneity property of the closed-loop system, which renders most existing homogeneity-based FOSMC techniques inapplicable [25].

Thus, given the constrained dynamical system (1), this study will investigate stability in the sense of uniform ultimate boundedness, which is in line with stability results for sliding mode regulation in adaptive control literature.

III. ADAPTIVE SLIDING MODE CONTROL DESIGN

In this section, an adaptive sliding mode control policy is designed that drives a nonlinear map-based transformed state variable to a small bound around the origin through online estimation and rejection of the uncertainty $\boldsymbol{\alpha}(t)$. To this end, we now invoke the following definition:

Definition 1: [30] For the multivariable signal $\boldsymbol{\xi}(t) \in \mathbb{R}^n$, assume that there exist positive constants ν_1, $\tilde{\nu}$ satisfying $\tilde{\nu} > \nu_1 > 0$, and that there exists a $T \geq 0$ and $\nu_2 > 0$ such that $||\boldsymbol{\xi}(t_0)|| \leq \nu_1$ implies

$$||\boldsymbol{\xi}(t)|| \leq \nu_2 \qquad \forall\, t \geq t_0 + T, \tag{2}$$

where ν_1 can be arbitrarily large. Then the signal $\boldsymbol{\xi}(t)$ is said to be uniformly ultimately bounded by the ultimate bound ν_2.

We then have the following Lemma characterizing the global uniform ultimate boundedness of $\boldsymbol{\xi}(t)$.

Lemma 1: [32] Let $V(\boldsymbol{\xi})$ be a continuously differentiable function such that

$$\begin{aligned} c_1 ||\boldsymbol{\xi}||^2 \leq V(\boldsymbol{\xi}) \leq c_2 ||\boldsymbol{\xi}||^2 \\ \dot{V}(\boldsymbol{\xi}) \leq -c_3 V(\boldsymbol{\xi}) \quad \forall ||\boldsymbol{\xi}|| \geq \nu_1, \end{aligned} \tag{3}$$

with $c_1, c_2, c_3 > 0$. Then, for a ball $\mathcal{B}$ of radius r, we define a positive constant $\sigma \leq \nu_1 \triangleq r(c_1/c_2)^{1/2}$. Then for every initial state $\boldsymbol{\xi}(t_0)$ satisfying $||\boldsymbol{\xi}(t_0)||^2 \leq \nu_1$, there exists a positive constant T such that the inequality (2) holds with $\nu_2 \triangleq \sigma(c_1/c_2)^{1/2}$, and ν_1 can be arbitrarily large.

A. STATE TRANSFORMATION

We now introduce the logistic function to initiate a nonlinear equality transformation $\boldsymbol{\Psi} : \mathbb{R}^n \to \mathbb{R}^n$ to map the constrained state, $\boldsymbol{x}(t)$, into an unconstrained variable $\boldsymbol{\zeta}(t) \in \mathbb{R}^n$ as,

$$\begin{aligned} \boldsymbol{x}(t) = \boldsymbol{\Xi}(\boldsymbol{\zeta}) \triangleq \boldsymbol{\delta}_1 + \boldsymbol{\Lambda}(\boldsymbol{\delta}_1, \boldsymbol{\delta}_2)\boldsymbol{\Psi}(\boldsymbol{\zeta}), \\ \boldsymbol{\Psi}(\boldsymbol{\zeta}) = [\psi(\zeta_1), .., \psi(\zeta_n)]^\top,\ \psi(\zeta_k) = \frac{e^{\zeta_k}}{1+e^{\zeta_k}}, \\ \boldsymbol{\Lambda}(\boldsymbol{\delta}_1, \boldsymbol{\delta}_2) = \mathrm{diag}[\delta_{2_k} - \delta_{1_k}],\ k = \{1, .., n\}. \end{aligned} \tag{4}$$

Note that the nonlinear transformation $\psi : (-\infty, \infty) \to (0, 1)$ is a smooth monotonically increasing function, and hence is invertible. It then follows that $\boldsymbol{x}(t) \in (\boldsymbol{\delta}_1, \boldsymbol{\delta}_2)$ $\forall\, \boldsymbol{\zeta}(t) \in \mathbb{R}^n$, thus requiring that the transformed variable $\boldsymbol{\zeta}(t)$ remain bounded in order to satisfy the state constraints $\forall t \geq 0$.

Moreover, as the components of the transformed state $\boldsymbol{\zeta}(t)$ can be expressed as

$$\zeta_k(t)=\psi^{-1}(x_k,\delta_{1_k},\delta_{2_k})=\ln\left(\frac{x_k-\delta_{1_k}}{\delta_{2_k}-x_k}\right),\ k=\{1,..,n\}, \quad (5)$$

we have $\boldsymbol{\zeta}(t) = \boldsymbol{\zeta}_0 = \left[\ln\left(-\frac{\delta_{1_1}}{\delta_{2_1}}\right),..,\ln\left(-\frac{\delta_{1_n}}{\delta_{2_n}}\right)\right]^\top$ when $\boldsymbol{x}(t)=\mathbf{0}$, so that the objective now translates to the synthesis of a control policy $\boldsymbol{u}(t)$ that drives a new unconstrained state error variable $\boldsymbol{\chi}(t)=\boldsymbol{\zeta}(t)-\boldsymbol{\zeta}_0$ to a uniform ultimate bound in finite time in the presence of uncertain parameters $\beta(\boldsymbol{\zeta},t)$, $\boldsymbol{\alpha}(\boldsymbol{\zeta},t)$.

Differentiating (4) and substituting in (1), we have,

$$\begin{aligned}
\dot{\boldsymbol{\zeta}}(t) &= \boldsymbol{g}(\boldsymbol{\zeta})\,\tilde{\boldsymbol{\alpha}}(\boldsymbol{\zeta},t)+\beta(\boldsymbol{\zeta},t)\boldsymbol{g}(\boldsymbol{\zeta})\boldsymbol{\Lambda}^{-1}\,\boldsymbol{\Phi}\boldsymbol{u}(t),\\
\tilde{\boldsymbol{\alpha}}(\boldsymbol{\zeta},t) &= \boldsymbol{\Lambda}^{-1}\boldsymbol{\alpha}(\boldsymbol{\zeta},t),\ \boldsymbol{g}(\boldsymbol{\zeta})=\left[\boldsymbol{\Psi}_\zeta(\boldsymbol{\zeta})\right]^{-1},\\
\boldsymbol{\Psi}_\zeta(\boldsymbol{\zeta}) &= \frac{\partial\boldsymbol{\Psi}(\boldsymbol{\zeta})}{\partial\boldsymbol{\zeta}}=\mathrm{diag}[\Psi_{\zeta_k}],\ \Psi_{\zeta_k}=\frac{e^{\zeta_k}}{(1+e^{\zeta_k})^2},\ k=1,..,n.
\end{aligned} \quad (6)$$

Note that the uncertainty term $\tilde{\boldsymbol{\alpha}}(\boldsymbol{\zeta},t)$ is now bounded by the unknown constant α^* satisfying $||\tilde{\boldsymbol{\alpha}}(\boldsymbol{\zeta},t)|| \le h(\boldsymbol{\zeta})\alpha^*$, with $h(\boldsymbol{\zeta}) = \max\{\alpha_0\circ\boldsymbol{\Xi}(\boldsymbol{\zeta}),1\} \ge 1$, $\alpha^* = ||\boldsymbol{\Lambda}^{-1}||\overline{\alpha}$. Consequently, observe that the uncertainty term $\boldsymbol{g}(\boldsymbol{\zeta})\tilde{\boldsymbol{\alpha}}(\boldsymbol{\zeta},t)$ in (6) has a state-dependent structure with coefficient $\boldsymbol{g}(\boldsymbol{\zeta})$ that is radially unbounded, thus necessitating the need for the synthesis of a state-dependent control policy that ensures finite-time convergence though continuous and bounded control action.

B. ADAPTIVE CONTROLLER DESIGN

Accordingly, the PI sliding variable $\boldsymbol{\sigma}(t)$ is defined as

$$\boldsymbol{\sigma}(t) = \boldsymbol{\chi}(t) + \boldsymbol{\Omega}\int_0^t \lceil\boldsymbol{\chi}(t)\rfloor^\mu\,dt, \quad (7)$$

where $\boldsymbol{\sigma}(t)\in\mathbb{R}^n$ is an available signal for feedback, $\boldsymbol{\Omega}\in\mathbb{R}^{n\times n}$ is a diagonal positive-definite matrix, and $0<\mu\le 1$. Note that the conventional PI sliding mode is recovered for $\mu=1$, while a non-singular terminal sliding mode is obtained for $0<\mu<1$ [33], [34]. Then, taking the time-derivative of (7) and using (6), we have,

$$\dot{\boldsymbol{\sigma}}(t)=\boldsymbol{g}(\boldsymbol{\zeta})\,\tilde{\boldsymbol{\alpha}}(\boldsymbol{\zeta},t)+\beta(\boldsymbol{\zeta},t)\boldsymbol{g}(\boldsymbol{\zeta})\,\boldsymbol{\Lambda}^{-1}\,\boldsymbol{\Phi}\boldsymbol{u}(t)+\boldsymbol{\Omega}\,\lceil\boldsymbol{\chi}(t)\rfloor^\mu. \quad (8)$$

Next, to tackle the state-dependent uncertainty term $\boldsymbol{g}(\boldsymbol{\zeta})\tilde{\boldsymbol{\alpha}}(\boldsymbol{\zeta},t)$ in (8), inspired by [30], we propose the following control law:

$$\begin{aligned}
\boldsymbol{u}(t) &= \underline{\beta}^{-1}\boldsymbol{\Phi}^{-1}\boldsymbol{\Lambda}\,\boldsymbol{\Psi}_\zeta(\boldsymbol{\zeta})\,\boldsymbol{v}(t),\ \boldsymbol{f}(\boldsymbol{\zeta})=\left[\boldsymbol{g}(\boldsymbol{\zeta})\quad -\boldsymbol{\Omega}\lceil\boldsymbol{\chi}\rfloor^\mu\right],\\
\boldsymbol{v}(t) &= -\boldsymbol{\Gamma}\boldsymbol{\sigma}-\overline{K}(t)\,h(\boldsymbol{\zeta})\,||\boldsymbol{f}(\boldsymbol{\zeta})||\,\mathrm{sat}(\boldsymbol{\sigma}/\varepsilon)-\boldsymbol{\Omega}\lceil\boldsymbol{\chi}\rfloor^\mu,\\
\dot{\overline{K}}(t) &= \eta\,h(\boldsymbol{\zeta})\,||\boldsymbol{\sigma}||\,||\boldsymbol{f}(\boldsymbol{\zeta})||-\rho\,\eta\,\overline{K}(t),\ \overline{K}(0)>0,
\end{aligned} \quad (9)$$

where $\boldsymbol{\Gamma}$ is a symmetric positive definite matrix, ε is a design constant chosen such that $0<\varepsilon\ll 1$, $\mathrm{sat}(\boldsymbol{y}/\varepsilon)$ is the saturation function

$$\mathrm{sat}(\boldsymbol{y}/\varepsilon)=\begin{cases}\boldsymbol{y}/\varepsilon & \text{if } ||\boldsymbol{y}||<\varepsilon\\ \lceil\boldsymbol{y}\rfloor^0 & \text{otherwise,}\end{cases} \quad (10)$$

and ρ, η are positive design constants.

C. STABILITY ANALYSIS

We now demonstrate that the trajectories of system (1) under the proposed control policy (9) achieve uniform finite-time convergence while simultaneously satisfying predefined state constraints as proof of the following theorem.

Theorem 1: Consider system (1) with an initial value such that the state $\boldsymbol{x}(0)$ is within the constraint region, i.e., $\boldsymbol{\delta}_1<\boldsymbol{x}(0)<\boldsymbol{\delta}_2$. Then, under Assumption 1, system (1) under the proposed adaptive control policy (9) achieves finite-time convergence of $\boldsymbol{\sigma}(t)$ to a uniform ultimate bound given by $\varpi=\sqrt{\frac{\rho q^{*2}}{\omega_1-\omega_2}}$, where $\omega_1\triangleq\frac{\min\{\lambda_{\min}\{\boldsymbol{\Gamma}\},\rho/2\}}{\max\{1/2,1/2\eta\}}>0$, $0<\omega_2<\omega_1$, $q^*=\alpha^*+\overline{\beta}/\underline{\beta}-1$, and $\gamma(\boldsymbol{\zeta},t)=\beta(\boldsymbol{\zeta},t)/\underline{\beta}-1$. Furthermore, control policy (9) ensures that the trajectories of system (1) lie within the full-state constraint set $\boldsymbol{\delta}_1<\boldsymbol{x}(t)<\boldsymbol{\delta}_2\ \forall\, t\ge 0$.

Proof: As a first step, note that $\boldsymbol{\zeta}(0)=\boldsymbol{\Psi}^{-1}(\boldsymbol{x}(0),\boldsymbol{\delta}_1,\boldsymbol{\delta}_2)$ is well-defined for $\boldsymbol{\delta}_1<\boldsymbol{x}(0)<\boldsymbol{\delta}_2$. The dynamics of $\boldsymbol{\zeta}(t)$ then evolves according to system (6) under the control policy (9). Then, by integrating the last equation in (9), we have,

$$\overline{K}(t)=e^{-\rho\eta t}\overline{K}(0)+\eta\int_0^t e^{-\rho\eta(t-\tau)}\,h(\boldsymbol{\zeta})||\boldsymbol{f}(\boldsymbol{\zeta})||\,||\boldsymbol{\sigma}||\,d\tau. \quad (11)$$

As $\overline{K}(0)>0$ and $h(\boldsymbol{\zeta})||\boldsymbol{f}(\boldsymbol{\zeta})||\,||\boldsymbol{\sigma}||\ge 0$, from (11), it can clearly be concluded that $\overline{K}(t)>0\,\forall\, t\ge 0$.

Now, to facilitate subsequent analysis, we consider the following Lyapunov function candidate

$$V=\frac{1}{2}\boldsymbol{\sigma}^\top\boldsymbol{\sigma}+\frac{1}{2\eta}[\overline{K}-q^*]^2. \quad (12)$$

Using (8) and (9), the time-derivative of (12) can be written as,

$$\begin{aligned}
\dot{V} &= \boldsymbol{\sigma}^\top\dot{\boldsymbol{\sigma}}+\frac{1}{\eta}[\overline{K}-q^*]\dot{\overline{K}}=\boldsymbol{\sigma}^\top\boldsymbol{g}(\boldsymbol{\zeta})\tilde{\boldsymbol{\alpha}}(\boldsymbol{\zeta},t)-\frac{\beta}{\underline{\beta}}\boldsymbol{\sigma}^\top\big[\boldsymbol{\Gamma}\boldsymbol{\sigma}\\
&\quad+\overline{K}h(\boldsymbol{\zeta})\,||\boldsymbol{f}(\boldsymbol{\zeta})||\,\mathrm{sat}(\boldsymbol{\sigma}/\varepsilon)+\boldsymbol{\Omega}\lceil\boldsymbol{\chi}\rfloor^\mu\big]+\boldsymbol{\sigma}^\top\boldsymbol{\Omega}\lceil\boldsymbol{\chi}\rfloor^\mu\\
&\quad+[\overline{K}-q^*][h(\boldsymbol{\zeta})\,||\boldsymbol{\sigma}||\,||\boldsymbol{f}(\boldsymbol{\zeta})||-\rho\overline{K}].
\end{aligned} \quad (13)$$

As $\beta(\boldsymbol{\zeta},t)\ge\underline{\beta}$, we introduce $\gamma(\boldsymbol{\zeta},t)=\beta(\boldsymbol{\zeta},t)/\underline{\beta}-1\ge 0$, so that from (13), we have,

$$\begin{aligned}
\dot{V} &= \boldsymbol{\sigma}^\top\boldsymbol{g}(\boldsymbol{\zeta})\tilde{\boldsymbol{\alpha}}(\boldsymbol{\zeta},t)-\boldsymbol{\sigma}^\top\boldsymbol{\Gamma}\boldsymbol{\sigma}-\overline{K}h(\boldsymbol{\zeta})||\boldsymbol{f}(\boldsymbol{\zeta})||\,\boldsymbol{\sigma}^\top\mathrm{sat}(\boldsymbol{\sigma}/\varepsilon)\\
&\quad-\gamma(\boldsymbol{\zeta},t)\big[\boldsymbol{\sigma}^\top\boldsymbol{\Gamma}\boldsymbol{\sigma}+\overline{K}\,h(\boldsymbol{\zeta})||\boldsymbol{f}(\boldsymbol{\zeta})||\,\boldsymbol{\sigma}^\top\mathrm{sat}(\boldsymbol{\sigma}/\varepsilon)\\
&\quad+\boldsymbol{\sigma}^\top\boldsymbol{\Omega}\lceil\boldsymbol{\chi}\rfloor^\mu\big]+[\overline{K}-q^*][h(\boldsymbol{\zeta})\,||\boldsymbol{\sigma}||\,||\boldsymbol{f}(\boldsymbol{\zeta})||-\rho\overline{K}].
\end{aligned} \quad (14)$$

We now introduce the auxiliary variable $\boldsymbol{q}(\boldsymbol{\zeta},t)=[\tilde{\boldsymbol{\alpha}}(\boldsymbol{\zeta},t)^\top,\gamma(\boldsymbol{\zeta},t)]^\top$, so that, by invoking the fact that $h(\boldsymbol{\zeta})\ge 1$, we have $||\boldsymbol{q}(\boldsymbol{\zeta},t)||\le h(\boldsymbol{\zeta})q^*$. Then, from (14),

$$\dot{V}=\boldsymbol{\sigma}^\top\boldsymbol{f}(\boldsymbol{\zeta})\boldsymbol{q}(\boldsymbol{\zeta},t)-\boldsymbol{\sigma}^\top\boldsymbol{\Gamma}\boldsymbol{\sigma}-\overline{K}\,h(\boldsymbol{\zeta})\,||\boldsymbol{f}(\boldsymbol{\zeta})||\,\boldsymbol{\sigma}^\top\mathrm{sat}(\boldsymbol{\sigma}/\varepsilon)$$

$$-\gamma(\boldsymbol{\zeta},t)\big[\boldsymbol{\sigma}^\top\boldsymbol{\Gamma}\boldsymbol{\sigma}+\overline{K}\,h(\boldsymbol{\zeta})\,||\boldsymbol{f}(\boldsymbol{\zeta})||\,\boldsymbol{\sigma}^\top\text{sat}(\boldsymbol{\sigma}/\varepsilon)\big] +[\overline{K}-q^*][h(\boldsymbol{\zeta})\,||\boldsymbol{\sigma}||\,||\boldsymbol{f}(\boldsymbol{\zeta})||-\rho\overline{K}]. \quad (15)$$

Using the definition of the saturation function, observe that $\gamma(\boldsymbol{\zeta},t)\big[\boldsymbol{\sigma}^\top\boldsymbol{\Gamma}\boldsymbol{\sigma}+\overline{K}\,h(\boldsymbol{\zeta})\,||\boldsymbol{f}(\boldsymbol{\zeta})||\,\boldsymbol{\sigma}^\top\text{sat}(\boldsymbol{\sigma}/\varepsilon)\big]\geq 0$, so that we have,

$$\begin{aligned}\dot{V}\leq&\boldsymbol{\sigma}^\top\boldsymbol{f}(\boldsymbol{\zeta})\boldsymbol{q}(\boldsymbol{\zeta},t)-\boldsymbol{\sigma}^\top\boldsymbol{\Gamma}\boldsymbol{\sigma}-\overline{K}\,h(\boldsymbol{\zeta})\,||\boldsymbol{f}(\boldsymbol{\zeta})||\,\boldsymbol{\sigma}^\top\text{sat}(\boldsymbol{\sigma}/\varepsilon)\\&+[\overline{K}-q^*][h(\boldsymbol{\zeta})\,||\boldsymbol{\sigma}||\,||\boldsymbol{f}(\boldsymbol{\zeta})||-\rho\overline{K}]\\\leq&||\boldsymbol{\sigma}||\,||\boldsymbol{f}(\boldsymbol{\zeta})||h(\boldsymbol{\zeta})\,q^*-\lambda_{\min}\{\boldsymbol{\Gamma}\}||\boldsymbol{\sigma}||^2-\rho[\overline{K}^2-\overline{K}q^*]\\&-\overline{K}\,h(\boldsymbol{\zeta})\,||\boldsymbol{f}(\boldsymbol{\zeta})||\,||\boldsymbol{\sigma}||+[\overline{K}-q^*]h(\boldsymbol{\zeta})||\boldsymbol{f}(\boldsymbol{\zeta})||\,||\boldsymbol{\sigma}||\\\leq&-\lambda_{\min}\{\boldsymbol{\Gamma}\}||\boldsymbol{\sigma}||^2-\rho[\overline{K}^2-\overline{K}q^*]. \quad (16)\end{aligned}$$

Then, using the fact that $\overline{K}^2-\overline{K}q^*\geq\frac{1}{2}[\overline{K}-q^*]^2-\frac{1}{2}q^{*2}$, we have from (16),

$$\begin{aligned}\dot{V}&\leq-\lambda_{\min}\{\boldsymbol{\Gamma}\}||\boldsymbol{\sigma}||^2-\frac{\rho}{2}[\overline{K}-q^*]^2+\frac{1}{2}\rho q^{*2}\\&\leq-\omega_1V+\frac{1}{2}\rho q^{*2}, \quad (17)\end{aligned}$$

where $\omega_1\triangleq\frac{\min\{\lambda_{\min}\{\boldsymbol{\Gamma}\},\rho/2\}}{\max\{1/2,1/2\eta\}}>0$. For the choice of a scalar ω_2 satisfying $0<\omega_2<\omega_1$, we have,

$$\begin{aligned}\dot{V}&\leq-\omega_2V-(\omega_1-\omega_2)V+\frac{1}{2}\rho q^{*2}\\&\leq-\omega_2V\forall\quad V\geq\Theta=\frac{\rho q^{*2}}{2(\omega_1-\omega_2)}. \quad (18)\end{aligned}$$

Clearly then, it follows directly from Lemma 1 that any trajectory enters the ball $\mathcal{V}=\big\{\{\boldsymbol{\sigma},\overline{K}\}\in\mathbb{R}^{n+1}|V\leq\Theta\big\}$ exponentially in finite-time and stays in $\mathcal{V}$ for all future time. Observe that the size of the ball can be made suitably small through a suitable choice of controller gains ρ,η and $\boldsymbol{\Gamma}$, so that by recognising that $V\geq\frac{1}{2}||\boldsymbol{\sigma}||^2$, we have the ultimate bound for $\boldsymbol{\sigma}(t)$ as $||\boldsymbol{\sigma}(t)||\leq\varpi=\sqrt{\frac{\rho q^{*2}}{\omega_1-\omega_2}}$. This bound is uniform as it is independent of initial conditions. Consequently, invoking Lemma 2 in [31], it can be concluded that this ultimate bound ϖ also holds for the unconstrained tracking error $\boldsymbol{\chi}(t)$, and it follows from (4) that $\boldsymbol{\delta}_1<\boldsymbol{x}(t)<\boldsymbol{\delta}_2$, so that state constraints are satisfied $\forall\,t\geq0$. This ends the proof. ■

Remark 2: Observe that the state-dependent uncertainty term $\boldsymbol{g}(\boldsymbol{\zeta})\tilde{\boldsymbol{\alpha}}(\boldsymbol{\zeta},t)$ arises as a natural consequence of employing the invertible transformation (4), and not as a result of structural knowledge as usually considered in adaptive control literature. In particular, the last two equations in (9) can estimate this state-dependent uncertainty term without imposing structural constraints on the perturbation term, which marks a major difference with the standard adaptive sliding mode control schemes in [16], [17], [18], [19], [20], and [21].

Remark 3: As noted earlier, the problem of controller synthesis for constrained nonlinear systems has been considered in [26], [27], and [28] with the objective of maximizing the attendant domain of attraction. However, as these studies only guarantee finite-time convergence in a small domain of attraction of the predefined region, it is apparent that these studies cannot be applied to the system considered in this study which is in contrast with the proposed scheme in this study that guarantees finite-time convergence from any initial condition located within the *predefined* state constraint set.

Remark 4: For the proposed scheme (9), parameters $\boldsymbol{\Omega}$ and μ determine the convergence time of the unconstrained error variable $\boldsymbol{\chi}(t)$, with a larger (resp. smaller) choice of $\boldsymbol{\Omega}$ (resp. μ) implying faster convergence of $\boldsymbol{\chi}(t)$ to the ultimate bound around the origin. Furthermore, as noted earlier, the size of this ultimate bound can be made sufficiently small for a smaller choice of gain parameter η, and a suitably large choice of parameters $\boldsymbol{\Gamma}$, ρ. However, an overly large choice of $\boldsymbol{\Gamma}$, $\boldsymbol{\Omega}$, ρ may result in a large control effort, while an overly small choice of μ, ε needs to be avoided in order to prevent control signal chattering.

Remark 5: In the absence of state constraints, note that the unconstrained conventional PI sliding variable $\tilde{\boldsymbol{\sigma}}(t)$ can be directly constructed as $\tilde{\boldsymbol{\sigma}}(t)=\boldsymbol{x}(t)+\boldsymbol{\Omega}\int_0^t\boldsymbol{x}(t)\,dt$. Consequently similar to (9), with $\tilde{h}(\boldsymbol{x})=\max\{\alpha_0(\boldsymbol{x}),1\}$, the alternative control policy for regulating the variable $\tilde{\boldsymbol{\sigma}}(t)$ (hence $\boldsymbol{x}(t)$) can be obtained as

$$\begin{aligned}&\boldsymbol{u}(t)=\underline{\beta}^{-1}\boldsymbol{\Phi}^{-1}\tilde{\boldsymbol{\nu}}(t),\ \tilde{\boldsymbol{f}}(\boldsymbol{x})=\big[\boldsymbol{I}\ -\boldsymbol{\Omega}\boldsymbol{x}\big],\\&\tilde{\boldsymbol{\nu}}(t)=-\boldsymbol{\Gamma}\tilde{\boldsymbol{\sigma}}-\overline{K}_1\tilde{h}(\boldsymbol{x})||\tilde{\boldsymbol{f}}(\boldsymbol{x})||\text{sat}\left(\frac{\tilde{\boldsymbol{\sigma}}}{\varepsilon}\right)-\boldsymbol{\Omega}\boldsymbol{x},\\&\dot{\overline{K}}_1(t)=\eta\tilde{h}(\boldsymbol{x})||\tilde{\boldsymbol{\sigma}}||\,||\tilde{\boldsymbol{f}}(\boldsymbol{x})||-\rho\eta\overline{K}_1(t),\ \overline{K}_1(0)>0. \quad (19)\end{aligned}$$

IV. BARRIER FUNCTION-BASED ADAPTIVE CONTROL

In the previous section, an adaptive control strategy is presented that guarantees state convergence to an ultimate bound in a finite-time. However, it is apparent that this ultimate bound ϖ is proportional to the magnitude of the external disturbance q^*, which is usually unknown *apriori*, and thus renders this strategy less desirable for implementation during practical applications. In order to overcome this drawback, an alternative control strategy is now proposed that relies on a barrier function to guarantee prescribed finite-time convergence to a small uniform ultimate bound that is independent of the magnitude of the external perturbation $\boldsymbol{q}(t)$. To this end, we now invoke the following Lemma.

Lemma 2: [35] Consider the differential equation

$$\dot{\varphi}(t)=-p(t)\varphi(t),\ p(t)=\frac{\dot{\vartheta}(t)}{1-\vartheta(t)+\iota}, \quad (20)$$

where $0<\iota\ll1$, and $\vartheta(t)$ satisfies the following properties:

(i) $\vartheta(t)$ is atleast C^2 on $(0,\infty)$.

(ii) $\vartheta(t)$ is continuous and non-decreasing on $[0,T_c]$, where $T_c<\infty$ is a predefined time instant. Also, we have $\vartheta(0)=0$, and $\vartheta(T_c)=1$.

(iii) $\dot{\vartheta}(0)=\dot{\vartheta}(T_c)=0$, $\vartheta(t)=1$ and $\dot{\vartheta}(t)=0\,\forall t\geq T_c$.

Then the system trajectory reaches the value $\frac{\iota}{1+\iota}\varphi(0)$ at time T_c.

A. ADAPTIVE BARRIER FUNCTION DESIGN

Then, inspired by [13], we propose the following control law to tackle the state-dependent uncertainty in (8):

$$\begin{aligned}
&\boldsymbol{u}(t) = \underline{\beta}^{-1}\boldsymbol{\Phi}^{-1}\boldsymbol{\Lambda}\,\boldsymbol{\Psi}_{\boldsymbol{\zeta}}(\boldsymbol{\zeta})\,\boldsymbol{w}(t),\ \dot{\boldsymbol{\kappa}}(t) = -\,p(t)\boldsymbol{\kappa}(t)\\
&\boldsymbol{w}(t) = -p(t)\boldsymbol{\kappa}(t) - K(t)\,h(\boldsymbol{\zeta})\,||\boldsymbol{f}(\boldsymbol{\zeta})||\,\lceil \boldsymbol{e}\rfloor^{0} - \boldsymbol{\Omega}\lceil \boldsymbol{\chi}\rfloor^{\mu},\\
&K(t) = \frac{\varrho\,||\boldsymbol{e}(t)||}{\tilde{\varepsilon} - ||\boldsymbol{e}(t)||},\ \boldsymbol{e}(t) = \boldsymbol{\sigma}(t) - \boldsymbol{\kappa}(t),
\end{aligned} \tag{21}$$

with $\boldsymbol{\kappa}(0) = \boldsymbol{\sigma}(0)$, ϱ and $\tilde{\varepsilon}$ are positive user-defined constants, and $\vartheta(t)$ in (20) is chosen as [13],

$$\vartheta(t) = \begin{cases} 10\big(\frac{t}{T_c}\big)^6 - 24\big(\frac{t}{T_c}\big)^5 + 15\big(\frac{t}{T_c}\big)^4 \text{ if } t \le T_c \\ 1 \quad t > T_c. \end{cases} \tag{22}$$

Observe that the controller gain $K(t)$ in (21) has a barrier function-like structure, so that $K(t)$ is a monotonically increasing function on $[0,\ \tilde{\varepsilon})$ that takes its minimum value at $\boldsymbol{e}(t) = \boldsymbol{0}$. Furthermore, note that we have $\boldsymbol{e}(0) = \boldsymbol{\chi}(0) - \boldsymbol{\kappa}(0) = \boldsymbol{0}$.

B. STABILITY ANALYSIS

We now demonstrate that the trajectories of system (1) under the proposed control policy (21) evolve within the predefined state constraint set, and achieve uniform convergence in a prescribed time T_c, as proof the following theorem.

Theorem 2: Consider system (1) with an initial value such that the state $\boldsymbol{x}(0)$ is within the constraint region, i.e., $\boldsymbol{\delta}_1 < \boldsymbol{x}(0) < \boldsymbol{\delta}_2$. Then, under Assumption 1, system (1) under the proposed adaptive control policy (21) achieves finite-time convergence of $\boldsymbol{\sigma}(t)$ to a uniform ultimate bound in prescribed time T_c, with the ultimate bound given by $\varpi_1 = \tilde{\varepsilon} + \frac{\iota}{1+\iota}||\boldsymbol{\sigma}(0)||$, and ensures satisfaction of the state constraint $\boldsymbol{\delta}_1 < \boldsymbol{x}(t) < \boldsymbol{\delta}_2\ \forall\, t \ge 0$.

Proof: As before, note that $\boldsymbol{\zeta}(0) = \boldsymbol{\Psi}^{-1}(\boldsymbol{x}(0), \boldsymbol{\delta}_1, \boldsymbol{\delta}_2)$ is well-defined for $\boldsymbol{\delta}_1 < \boldsymbol{x}(0) < \boldsymbol{\delta}_2$. The dynamics of $\boldsymbol{\zeta}(t)$ then evolves according to system (6) under the control policy (21).

To facilitate subsequent analysis, we consider the following Lyapunov function candidate

$$W = \frac{1}{2}\boldsymbol{e}^{\top}\boldsymbol{e}. \tag{23}$$

Using (8) and (21), the time-derivative of (23) can be written as,

$$\begin{aligned}
\dot{W} = \boldsymbol{e}^{\top}[\dot{\boldsymbol{\sigma}} - \dot{\boldsymbol{\kappa}}] = \boldsymbol{e}^{\top}\big[\boldsymbol{g}(\boldsymbol{\zeta})\tilde{\boldsymbol{\alpha}}(\boldsymbol{\zeta}, t) + \boldsymbol{\Omega}\lceil \boldsymbol{\chi}\rfloor^{\mu} + p(t)\boldsymbol{\kappa}(t)\big]\\
-\frac{\beta}{\underline{\beta}}\boldsymbol{e}^{\top}\big[p(t)\boldsymbol{\kappa}(t) + K(t)\,h(\boldsymbol{\zeta})\,||\boldsymbol{f}(\boldsymbol{\zeta})||\,\lceil \boldsymbol{e}\rfloor^{0} + \boldsymbol{\Omega}\lceil \boldsymbol{\chi}\rfloor^{\mu}\big].
\end{aligned} \tag{24}$$

Then, invoking the fact that $\gamma(\boldsymbol{\zeta}, t) = \beta(\boldsymbol{\zeta}, t)/\underline{\beta} - 1 \ge 0$, we have,

$$\begin{aligned}
\dot{W} &= \boldsymbol{e}^{\top}\big[\boldsymbol{g}(\boldsymbol{\zeta})\tilde{\boldsymbol{\alpha}}(\boldsymbol{\zeta}, t) - K(t)\,h(\boldsymbol{\zeta})\,||\boldsymbol{f}(\boldsymbol{\zeta})||\,\lceil \boldsymbol{e}\rfloor^{0}\big]\\
&\quad - \gamma(\boldsymbol{\zeta}, t)\boldsymbol{e}^{\top}\big[p(t)\boldsymbol{\kappa}(t) + K(t)\,h(\boldsymbol{\zeta})\,||\boldsymbol{f}(\boldsymbol{\zeta})||\,\lceil \boldsymbol{e}\rfloor^{0} + \boldsymbol{\Omega}\lceil \boldsymbol{\chi}\rfloor^{\mu}\big]\\
&\le \boldsymbol{e}^{\top}\big[\boldsymbol{f}(\boldsymbol{\zeta})\boldsymbol{q}(\boldsymbol{\zeta}, t) - K(t)\,h(\boldsymbol{\zeta})\,||\boldsymbol{f}(\boldsymbol{\zeta})||\,\lceil \boldsymbol{e}\rfloor^{0}\big]\\
&\quad - \gamma(\boldsymbol{\zeta}, t)\boldsymbol{e}^{\top}\big[p(t)\boldsymbol{\kappa}(t) + K(t)\,h(\boldsymbol{\zeta})\,||\boldsymbol{f}(\boldsymbol{\zeta})||\,\lceil \boldsymbol{e}\rfloor^{0}\big].
\end{aligned} \tag{25}$$

Observe that from (22), we have $0 \le \vartheta(t) \le 1$, so that from Lemma 2, it follows that $p(t) \ge 0$. Then, from (21), we have $\boldsymbol{\kappa}(t) = e^{-\int_0^t p(t)\,dt}\boldsymbol{\kappa}(0)$, so that $||\boldsymbol{\kappa}(t)|| \le ||\boldsymbol{\kappa}(0)||$. Consequently, there exists a positive constant p^* satisfying $p^* = \sup_t\{p(t)\,||\boldsymbol{\kappa}(t)||\}$. Then, using the fact that $h(\boldsymbol{\zeta})||\boldsymbol{f}(\boldsymbol{\zeta})|| \ge h(\boldsymbol{\zeta})||\boldsymbol{g}(\boldsymbol{\zeta})|| \ge 1$, we have from (25),

$$\begin{aligned}
\dot{W} &\le -[K(t) - q^*]\,h(\boldsymbol{\zeta})\,||\boldsymbol{f}(\boldsymbol{\zeta})||\,||\boldsymbol{e}||\\
&\quad - \gamma(\boldsymbol{\zeta}, t)\big[K(t)\,h(\boldsymbol{\zeta})\,||\boldsymbol{f}(\boldsymbol{\zeta})|| - \sup_t\{p(t)||\boldsymbol{\kappa}(t)||\}\big]\,||\boldsymbol{e}||\\
&\le -[K(t) - q^*]\,||\boldsymbol{e}|| - \gamma(\boldsymbol{\zeta}, t)[K(t) - p^*]\,||\boldsymbol{e}||.
\end{aligned} \tag{26}$$

Then, using (21) and (26), we can derive that $\dot{W} \le 0$ provided $||\boldsymbol{e}(t)|| \ge \frac{\tilde{q}\tilde{\varepsilon}}{\varrho + \tilde{q}}$, with $\tilde{q} = \max\{p^*,\ q^*\}$. Thus, it follows that $||\boldsymbol{e}(t)|| \le \frac{\tilde{q}\tilde{\varepsilon}}{\varrho + \tilde{q}} < \tilde{\varepsilon}$ for all $t \ge 0$ as $\boldsymbol{e}(0) = \boldsymbol{0}$.

Furthermore, using Lemma 2, it follows that the auxiliary variable $\boldsymbol{\kappa}(t)$ attains the value of $\frac{\iota}{1+\iota}\boldsymbol{\sigma}(0)$ for all $t \ge T_c$. As $||\boldsymbol{\sigma}(t)|| \le ||\boldsymbol{e}(t)|| + ||\boldsymbol{\kappa}(t)||$, we have

$$||\boldsymbol{\sigma}(t)|| \le \varpi_1 = \tilde{\varepsilon} + \frac{\iota}{1+\iota}||\boldsymbol{\sigma}(0)|| \qquad \forall\, t \ge T_c. \tag{27}$$

As ι is a very small positive constant, the second term in (27) can be neglected, so that the ultimate bound ϖ_1 is independent of the magnitude of the size of the disturbance q^*. Furthermore, this bound is now uniform as it is independent of initial conditions. Consequently, as before, as the state variable $\boldsymbol{\zeta}(t)$ converges in a finite-time to this small bound around $\boldsymbol{\zeta}_0$, it follows from (4) that $\boldsymbol{\delta}_1 < \boldsymbol{x}(t) < \boldsymbol{\delta}_2$, so that the state constraints are satisfied $\forall\, t \ge 0$. This ends the proof. ■

Remark 6: From the previous analysis, it is clear that for the proposed scheme (21), the gain parameters ϱ (resp. $\tilde{\varepsilon}$) may be chosen to be suitably large (resp. suitably small) to ensure convergence to an arbitarily small bound. As before, the parameter $\boldsymbol{\Omega}$ (resp. μ) may be chosen to be suitably large (resp. small) to ensure faster convergence of the unconstrained error $\boldsymbol{\chi}(t)$ to the ultimate bound around the origin. Furthermore, prescribing an overly small convergence time T_c may impose a large control effort, while overly small values of $\tilde{\varepsilon}$ and μ may result in control signal chattering.

Remark 7: Note that the adaptive barrier-function based strategy (21) behaves differently from [12] in two key aspects: (i) it avoids introducing a discontinuity at $\boldsymbol{e}(t) = 0$, and (ii) prescribed-time convergence is achieved by relying on the time-based generator system (20) that precludes the need for adopting a switching gain strategy. Thus, in contrast with the barrier function based strategy in [12], this policy realizes prescribed-time convergence of the error through smooth and bounded control action that alleviates chattering, while remaining bounded at the prescribed time T_c.

Remark 8: In contrast with prevalent sliding mode control schemes in adaptive control literature, note that the last two equations in (21) provide online adaptation and rejection of

the state-dependent disturbance term $\boldsymbol{g}(\boldsymbol{\zeta})\tilde{\boldsymbol{\alpha}}(\boldsymbol{\zeta}, t)$. In particular, unlike the adaptive schemes proposed in [11], [12], and [31], the adaptive barrier function strategy assures uniform convergence in user-prescribed finite time to a perturbation-independent ultimate bound ϖ_1. If the trajectory were to escape the bound ϖ_1 in response to a sudden change in the perturbation signal $\boldsymbol{\alpha}(\boldsymbol{x}, t)$, a straightforward time-resetting scheme, similar to the strategy considered in [13], may be adopted to ensure that the system trajectory converges to this ultimate bound again within the predefined time T_c.

Remark 9: It is evident that the proposed policy (21) inherits all the advantages of the barrier function-based strategy in [13] while tackling the key drawback of not accounting for the state-dependent structure of the perturbation term $\boldsymbol{\alpha}(\boldsymbol{x}, t)$, which becomes critical to realizing bounded control action for achieving prescribed-time prescribed-bound convergence in the face of an unknown exogenous disturbance, as demonstrated in the current study.

V. EXPERIMENTAL VALIDATION

In this section, the problem of accomplishing visual formation control is used to experimentally validate the proposed strategies, and a performance comparison study with the controllers in [1], [12], [13], and [31] is used to highlight the advantages of the proposed schemes.

A. IMAGE-PLANE FORMATION KINEMATICS

Consider the motion of a pair of leader-follower robots with the leader R_i and the follower R_j (Fig. 1(a)). The kinematics of the k^{th} velocity-controlled robot R_k ($k \in \{i, j\}$) is given as $\dot{x}_k = b_k \cos\theta_k$, $\dot{y}_k = b_k \sin\theta_k$, $\dot{\theta}_k = \omega_k$, where $r_k = [x_k, y_k]^\top$ and θ_k are respectively the position and orientation of the robot R_k in a fixed reference frame, b_k and w_k are respectively the linear and angular velocities of the robot in the body-fixed reference frame $\mathcal{B}_k = [x_{bk}, y_{bk}, z_{bk}]^\top$. The relative position of the leader R_i with respect to the follower frame $\mathcal{B}_j$ is then given by [1]:

$$\boldsymbol{r}_{ij} = \begin{bmatrix} x_{ij} \\ y_{ij} \end{bmatrix} = \begin{bmatrix} \cos\theta_j & \sin\theta_j \\ -\sin\theta_j & \cos\theta_j \end{bmatrix} (\boldsymbol{r}_i - \boldsymbol{r}_j) \tag{28}$$

Taking the time derivative of (28), we have,

$$\dot{\boldsymbol{r}}_{ij} = [b_i \cos\theta_{ij} - b_j + y_{ij}\omega_j,\ b_i \sin\theta_{ij} - x_{ij}\omega_j]^\top \tag{29}$$

where $\theta_{ij} = \theta_i - \theta_j$ is the relative orientation between the leader and the follower.

The follower robot R_j is now equipped with a forward-looking perspective camera mounted on the follower robot. The reference frame is given by $\mathcal{C}_j = \{x_{cj}, y_{cj}, z_{cj}\}$, with the optical centre of the camera located at the origin of the reference frame $\mathcal{B}_j$, the camera's positive vertical axis pointing straight up and perpendicular to the ground plane, and the camera's optical axis (z_{cj}-axis) aligned with the x_{bj} axis as shown in Fig. 1(a). The normalized image-plane coordinates of a single point feature P rigidly located on the leader robot R_i are then given by $\boldsymbol{\pi} = [u_{ij}, v_{ij}]^\top = [\frac{y_{ij}}{x_{ij}}, \frac{z_i}{x_{ij}}]^\top$. Finally, the image plane formation kinematics can be derived as [1],

$$\dot{\boldsymbol{\pi}} = \beta \boldsymbol{\Phi} \boldsymbol{u}(t) + \boldsymbol{\alpha}(\boldsymbol{\pi}, t),\ \boldsymbol{u}(t) = [b_{\text{cmd}}, \omega_{\text{cmd}}]^\top,\ \dot{\theta}_{ij} = \omega_i - \omega_j,$$
$$\boldsymbol{\alpha} = \begin{bmatrix} \sin\theta_{ij} - u_{ij}\cos\theta_{ij} \\ -v_{ij}\cos\theta_{ij} \end{bmatrix} \frac{v_{ij}}{z_i} b_i,\ \boldsymbol{\Phi} = \begin{bmatrix} u_{ij}\frac{v_{ij}}{z_i} & -u_{ij}^2 - 1 \\ \frac{v_{ij}^2}{z_i} & -u_{ij}v_{ij} \end{bmatrix}. \tag{30}$$

where b_{cmd}, ω_{cmd} are the linear and angular velocity commands supplied to the follower robot. The parameter $\beta(t)$ is used to account for the internal dynamics of the follower robot which is usually modeled as a first-order system with an input-delay [36], so that we have $\beta(t) \geq \underline{\beta} = \min\{\inf_t[b_j/b_{\text{cmd}}], \inf_t[\omega_j/\omega_{\text{cmd}}]\}$. Detailed calibration tests are undertaken by recording the follower robot's velocity data in response to reference step commands, which are shown in Fig. 2. Clearly, from this figure, it is apparent that $\underline{\beta} = 0.5$.

For practical perspective systems, it is reasonable to assume that the point feature is located ahead of the camera, so that $x_{ij} > 0$. Furthermore, we have $z_i \neq 0$, so that $v_{ij} = z_i/x_{ij} \neq 0$. Thus, the determinant of $\boldsymbol{\Phi}$ satisfies $\text{Det}[\boldsymbol{\Phi}] = v_{ij}^2/z_i \neq 0$, ensuring that the matrix $\boldsymbol{\Phi}$ is invertible. Furthermore, note that $||\boldsymbol{\alpha}(\boldsymbol{\pi}, t)|| \leq \alpha_0(\boldsymbol{\pi})\overline{\alpha}$, where $\alpha_0(\boldsymbol{\pi}) = |v_{ij}|\sqrt{1 + u_{ij}^2 + v_{ij}^2}$ is available for feedback, and $\overline{\alpha} = \sup_t\{|b_i(t)|\}/|z_i|$ is unknown.

Then, given the desired formation pattern $\boldsymbol{r}_{ij}^d = \left[x_{ij}^d, y_{ij}^d\right]^\top$ and the corresponding desired coordinates $\boldsymbol{\pi}^d = [u_{ij}^d, v_{ij}^d]^\top = \left[y_{ij}^d/x_{ij}^d, z_i/x_{ij}^d\right]$, control policies (9), (21) are used to synthesize $\boldsymbol{u}(t)$ that drive the image-plane error $\Delta\boldsymbol{\pi} = [\Delta u_{ij}, \Delta v_{ij}]^\top := \boldsymbol{\pi} - \boldsymbol{\pi}^d$ (thus formation error $\Delta\boldsymbol{r}_{ij} = [\Delta x_{ij}, \Delta y_{ij}]^\top$) to a small bound around the origin in a finite time in the presence of uncertainty $\boldsymbol{\alpha}(\boldsymbol{\pi}, t)$ and visibility constraints $u^- \leq u_{ij} \leq u^+$, $v^- \leq v_{ij} \leq v^+$, where u^-, u^+, v^-, v^+ are known constants.

B. EXPERIMENTAL SETUP

Figure 1(b) depicts the experimental setup consisting of the Qualisys® motion capture system, a ground station, and a leader robot with a fiducial marker as the feature to be tracked, and a follower with a monocular camera. In these experiments, the centroid of an Aruco marker pattern is used as a binary fiducial marker, which is detected and tracked in a manner similar to [37]. The motion capture system obtains the ground truth trajectories of the leader and the follower in the global reference frame. An Intel RealSense D435i camera is used to obtain 640 × 480 grayscale images that are subsequently used to detect and track the fiducial marker to accomplish formation control onboard. The height of the centroid of the feature pattern is computed as 0.25 m, and the focal length of the camera is 610.5 pixels. The normalized image-plane coordinates are then directly obtained using the above procedure as $\boldsymbol{\pi}^d = [-0.016, 0.17]^\top$. The adaptive controller and the image processing algorithm are directly implemented on the onboard computer of the follower robot,

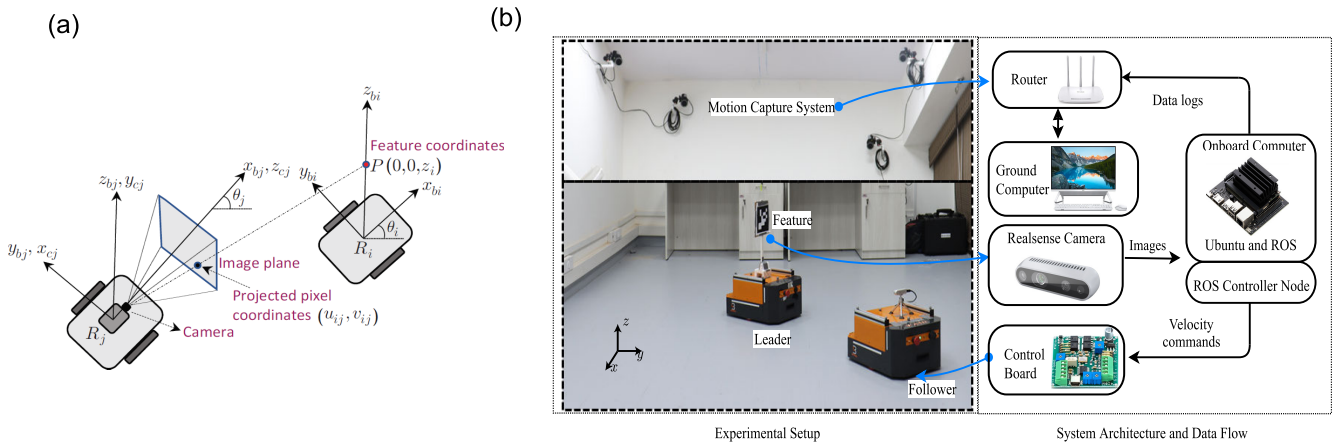

FIGURE 1. (a) Planar coordinate definition and perspective vision system diagram. (b) Experimental setup, system architecture and the data flow diagram.

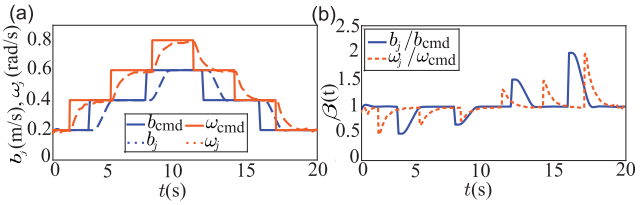

FIGURE 2. Time-trajectory of linear and angular velocity, and the corresponding command inputs.

with the camera images and feedback loop running at a frequency of 30 Hz. The control algorithm is written in Python and implemented on a setup comprising the Robot Operating System (ROS) Melodic framework running on Ubuntu 18.04.

C. RESULTS AND DISCUSSION

The experimental results are obtained using different controllers for a circular trajectory for two different cases of the leader's velocity profile:

- Constant leader velocity of $b_i = 0.1$ m/s, $\omega_i = 0.07$ rad/s
- leader velocity varies $b_i = 0.1 \rightarrow 0.25$ m/s, $\omega_i = 0.07 \rightarrow 0.17$ rad/s at $t = 39$ s.

For this setup, the visibility bounds are directly obtained as $\boldsymbol{\delta}_1 = [-0.38, -0.47]^\top$, $\boldsymbol{\delta}_2 = [0.40, 0.11]^\top$. Figures 3, 4 depict the results obtained with the proposed scheme (9) for the two different cases of varying leader velocity with gain parameters chosen as $\boldsymbol{\Omega} = 0.2\boldsymbol{I}$, $\boldsymbol{\Gamma} = 0.0005\boldsymbol{I}$, $\eta = 0.025$, $\rho = 500$, $\varepsilon = 0.1$, $\overline{K}(0) = 0.01$, $\mu = 1$. From Figs. 3(a)-(c), it is evident that formation errors in configuration space and in the image-plane nearly converge to the origin in a finite time under continuous and bounded control action (Fig. 3(d)). Note that these conclusions hold true even when a sharp and significant discontinuity in the perturbation term $\boldsymbol{\alpha}(\boldsymbol{\pi}, t)$ is introduced, as is the case with the varying leader velocity profile (Fig. 4).

Figures 5, 6 depict the results obtained with the proposed scheme (21) for the two different cases of varying leader velocity with gain parameters chosen as $\boldsymbol{\Omega} = 0.1\boldsymbol{I}$, $\iota = 0.1$, $\tilde{\varepsilon} = 1$, $\varrho = 0.015$, $\mu = 1$. The prescribed convergence time is chosen as $T_c = 10$ seconds. From Fig. 5(a)-(c), it is again evident that controller (21) drives the formation errors nearly to the origin under continuous and bounded control action (Fig. 5(d)). As before, the controller ensures that the formation errors are driven to the origin even in the presence of a significant change in the perturbation term arising from the abrupt change in the leader's velocity profile (Fig. 6).

Figure 7 depicts the results obtained with the alternative scheme (19) with gain parameters chosen the same as in proposed scheme (9). However, in contrast with previous cases, the absence of enforcement of state constraints in this case results in controller (19) driving the formation errors away from the origin, thus leading to the violation of the visibility constraint and resulting in the loss of feature tracking and formation control. Thus, this highlights the importance of the synthesis of the proposed strategies under the nonlinear mapping (4) that ensures that the formation control objective is achieved by ensuring satisfaction of the visibility constraints during the tracking process.

Finally, in order to further illustrate the advantages of the proposed schemes, experimental results are also obtained with the (i) prescribed-time prescribed-bound (PTPB) barrier function-based controller [13], (ii) the adaptive PI control scheme in [31], (iii) the alternative barrier function-based adaptive controller scheme [12], and (iv) the prescribed performance controller (PPC) [1]. Note that the adaptive schemes in [12] and [13] do not admit state constraints as well as the state-dependent structure of the perturbation term $\boldsymbol{\alpha}(\boldsymbol{\pi}, t)$. For the controller in [13], the gain parameters are chosen as

$$\text{PTPB}: \alpha = 0.06,\ T_c = 1,\ \epsilon = 0.18,\ \kappa = 0.1,\ \Theta = 1.$$

For the controller in [31], the gain parameters are chosen as

$$\text{Adaptive PI}: \overline{K}_p = 0.05,\ \beta = 0.1,\ \iota = 0.5,\ \sigma = 0.1,\ \gamma = 0.05,\ \eta_0 = 0.5,\ \eta_\infty = 0.25,\ a_0 = 0.5.$$

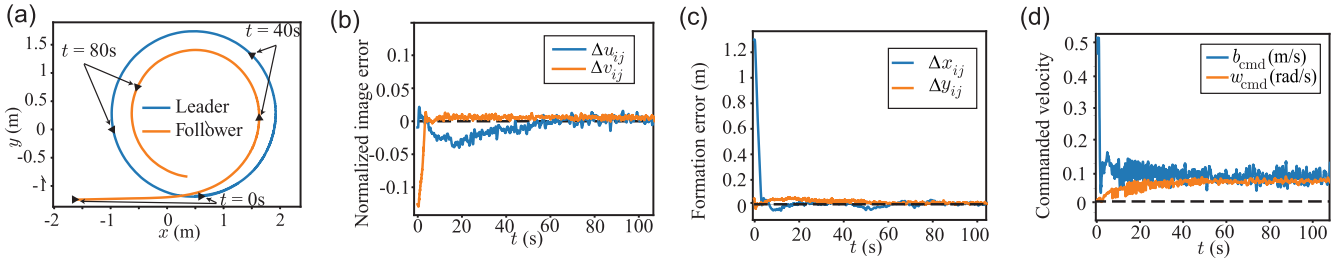

FIGURE 3. Experimental results obtained with proposed controller (9) for the constant velocity case and $\mu = 1$. (a) Leader and follower trajectories with snapshots provided every 40 seconds. (b) Time-trajectories of normalized image-plane formation errors. (c) Time-trajectories of formation errors in configuration space. (d) Control commands executed by the follower robot.

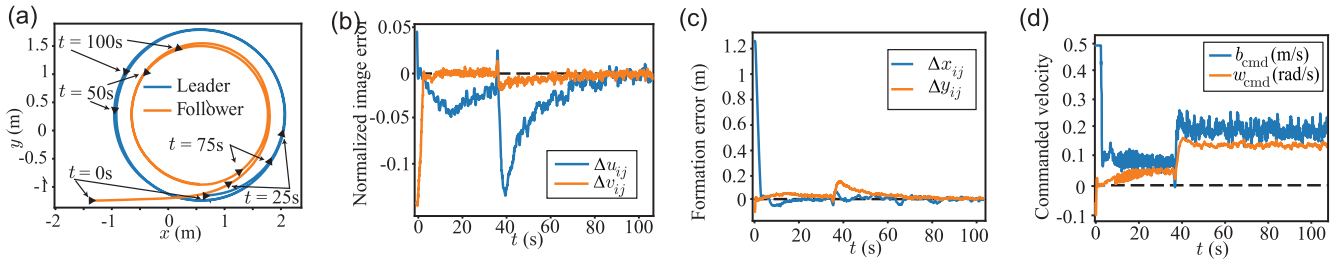

FIGURE 4. Experimental results obtained with proposed controller (9) for the varying velocity case and $\mu = 1$. (a) Leader and follower trajectories with snapshots provided every 25 seconds. (b) Time-trajectories of normalized image-plane formation errors. (c) Time-trajectories of formation errors in configuration space. (d) Control commands executed by the follower robot.

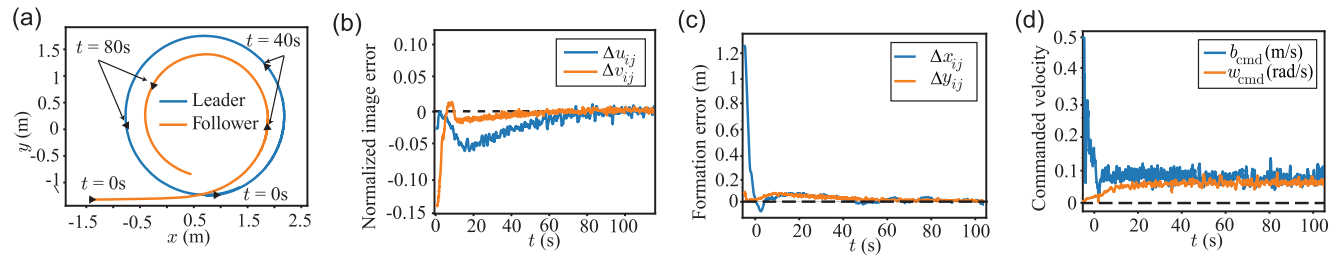

FIGURE 5. Experimental results obtained with proposed controller (21) for the constant velocity case and $\mu = 1$. (a) Leader and follower trajectories with snapshots provided every 40 seconds. (b) Time-trajectories of normalized image-plane formation errors. (c) Time-trajectories of formation errors in configuration space. (d) Control commands executed by the follower robot.

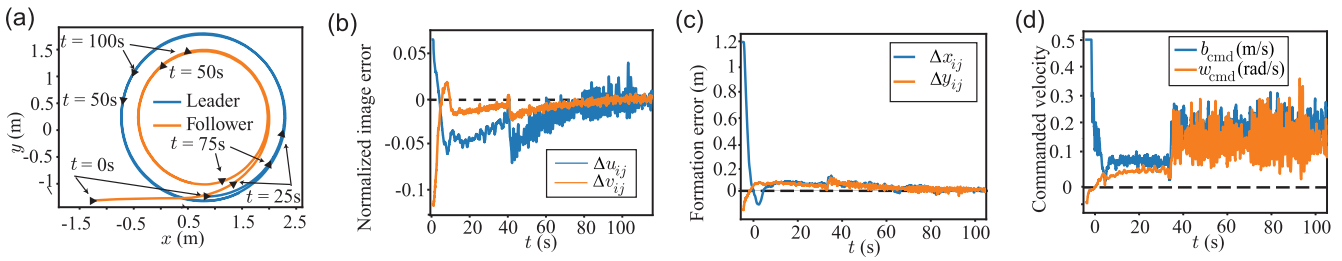

FIGURE 6. Experimental results obtained with proposed controller (21) for the varying velocity case and $\mu = 1$. (a) Leader and follower trajectories with snapshots provided every 25 seconds. (b) Time-trajectories of normalized image-plane formation errors. (c) Time-trajectories of formation errors in configuration space. (d) Control commands executed by the follower robot.

For the controller in [1], the gain parameters are chosen as

$$\text{PPC}: \ K_1{=}\text{diag}[0.1, 0.16], \ K_2{=}\text{diag}[0.0025, 0.001], \\ \rho_\infty = 0.1, \ l = 0.2.$$

For [12], the controller structure is given by $\boldsymbol{u}(t) = -\boldsymbol{\Phi}^{-1}[K_u \text{sign}(\Delta u_{ij}), K_v \text{sign}(\Delta v_{ij})]^\top$, with the adaptive gains given by

$$K_a(t){=}\begin{cases} \gamma_a, \ \dot{\gamma}_a{=}12.2|\Delta a_{ij}(t)|, & \text{if } |\Delta a_{ij}| > \epsilon_a/2 \\ \dfrac{\epsilon_a F_a}{\epsilon_a - |\Delta a_{ij}|}, & \text{otherwise}, \ a{=}\{u, v\}. \end{cases}$$

The gain parameters are chosen as $\gamma_u(0) = 15$, $\gamma_v(0) = 10$, $\epsilon_u = 0.08$, $\epsilon_v = 0.03$, $F_u = 17$, and $F_v = 9$.

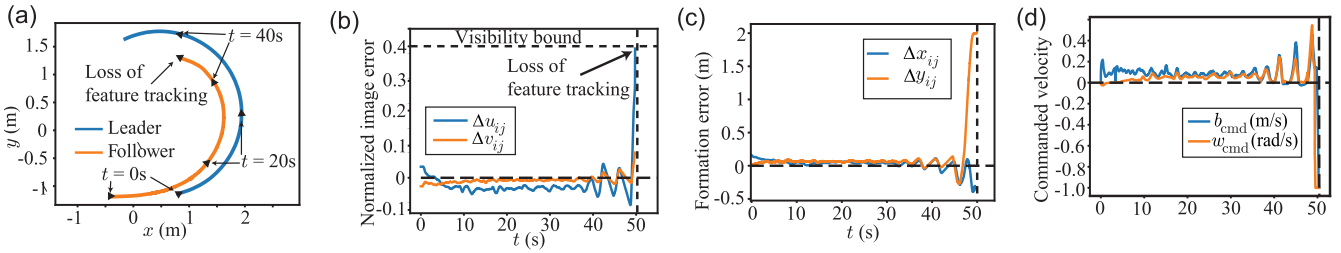

FIGURE 7. Experimental results obtained with controller (19) without visibility constraints for the constant velocity case. (a) Leader and follower trajectories with snapshots provided every 20 seconds. (b) Time-trajectories of normalized image-plane formation errors with vertical dashed line denoting the instant of loss of feature tracking and formation control due to violation of visibility constraint. (c) Time-trajectories of formation errors in configuration space. (d) Control commands executed by the follower robot.

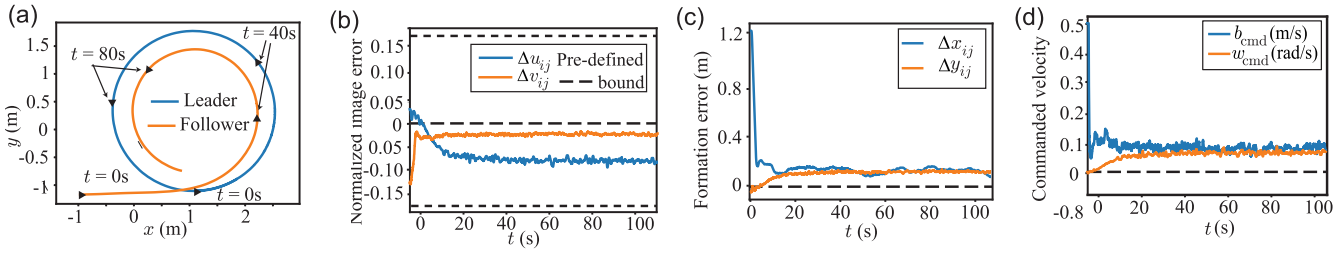

FIGURE 8. Experimental results obtained with the PTPB controller [13] for the constant velocity case. (a) Leader and follower trajectories with snapshots provided every 40 seconds. (b) Time-trajectories of normalized image-plane formation errors. (c) Time-trajectories of formation errors in configuration space. (d) Control commands executed by the follower robot.

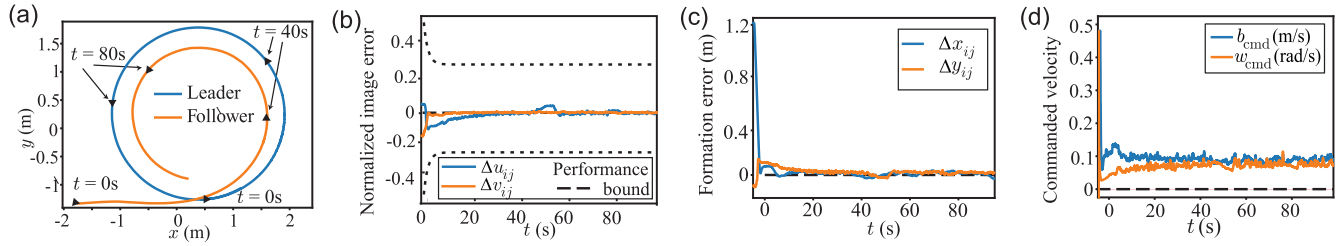

FIGURE 9. Experimental results obtained with the adaptive PI controller in [31] for the constant velocity case. (a) Leader and follower trajectories with snapshots provided every 40 seconds. (b) Time-trajectories of normalized image-plane formation errors. (c) Time-trajectories of formation errors in configuration space. (d) Control commands executed by the follower robot.

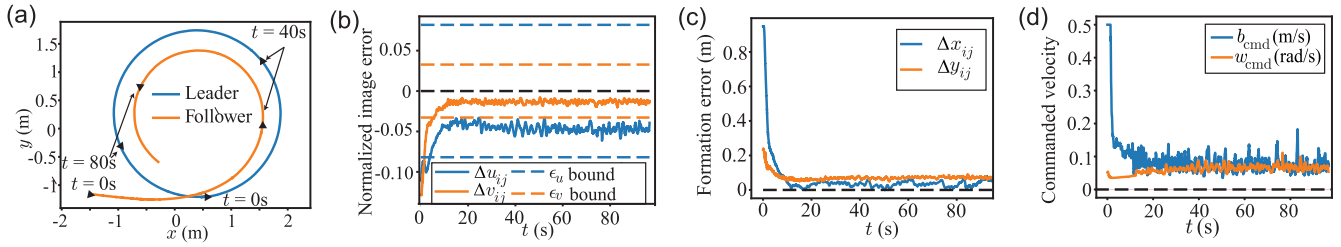

FIGURE 10. Experimental results obtained with barrier function-based controller [12] for the constant velocity case. (a) Leader and follower trajectories with snapshots provided every 40 seconds. (b) Time-trajectories of normalized image-plane formation errors. (c) Time-trajectories of formation errors in configuration space. (d) Control commands executed by the follower robot.

Figures 8-11 depict the results obtained using these schemes for the constant leader velocity case. For the case of the varying leader velocity profile, the control schemes [1], [12], [31] lead to *formation divergence* (Figs. 13-15), whereas the PTPB control scheme [13] is able to accomplish formation control only at the cost of sustaining large errors in steady-state (Fig. 12). Table 1 shows the statistical values of the steady-state root-mean square error (RMSE) and mean absolute percentage error (MAPE) metrics of the formation error in configuration space, as well as the control input

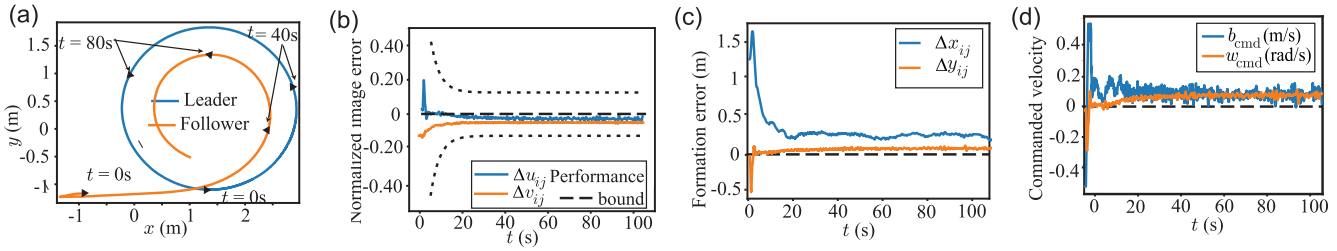

FIGURE 11. Experimental results obtained with the comparison controller in [1] for the constant velocity case. (a) Leader and follower trajectories with snapshots provided every 40 seconds. (b) Time-trajectories of normalized image-plane formation errors. (c) Time-trajectories of formation errors in configuration space. (d) Control commands executed by the follower robot.

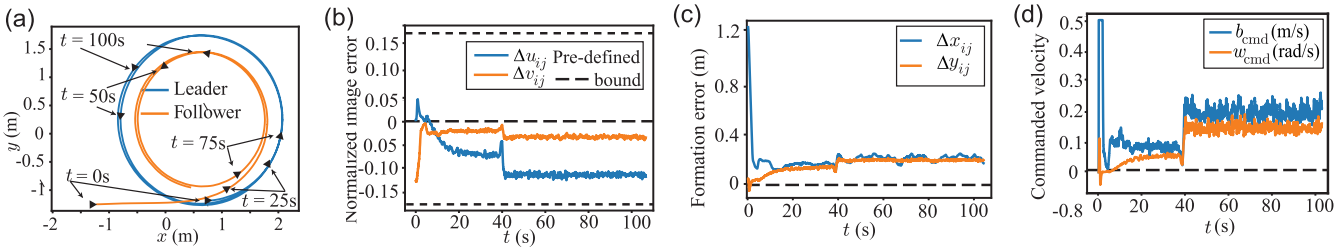

FIGURE 12. Experimental results obtained with the PTPB controller [13] for the varying velocity case. (a) Leader and follower trajectories with snapshots provided every 25 seconds. (b) Time-trajectories of normalized image-plane formation errors. (c) Time-trajectories of formation errors in configuration space. (d) Control commands executed by the follower robot.

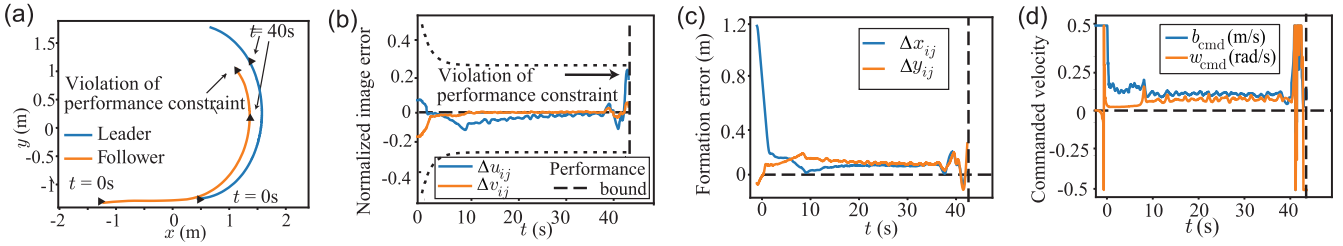

FIGURE 13. Experimental results obtained with the adaptive PI controller in [31] for the varying velocity case. (a) Leader and follower trajectories with snapshots provided every 40 seconds. (b) Time-trajectories of normalized image-plane formation errors with vertical dashed line denoting the instant of loss of feature tracking and formation control due to violation of performance constraint. (c) Time-trajectories of formation errors in configuration space. (d) Control commands executed by the follower robot.

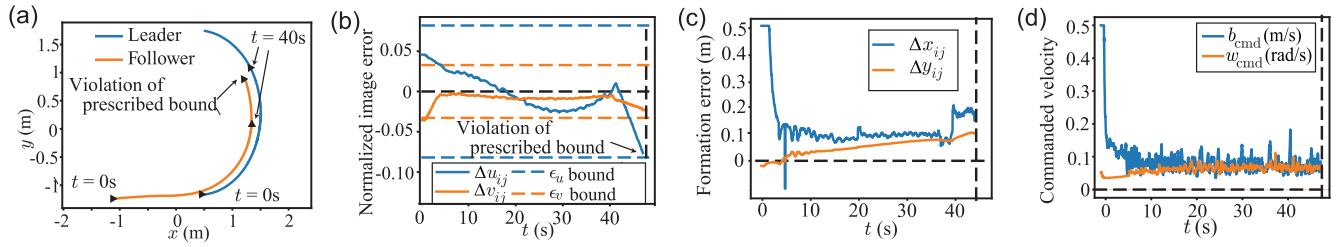

FIGURE 14. Experimental results obtained with barrier function-based controller [12] for the varying velocity case. (a) Leader and follower trajectories with snapshots provided every 40 seconds. (b) Time-trajectories of normalized image-plane formation errors with vertical dashed line denoting the instant of loss of feature tracking and formation control due to violation of prescribed bound. (c) Time-trajectories of formation errors in configuration space. (d) Control commands executed by the follower robot.

metrics which are computed using various controllers over the last 20 seconds of robot motion. The error metrics for the proposed schemes are obtained for both the conventional PI sliding mode ($\mu = 1$) and the terminal non-singular sliding mode ($\mu = 0.75$). Clearly, the steady-state performance of the adaptive strategy (9) is superior to the adaptive barrier function-based controller scheme (21). Moreover, for both these control schemes, formation errors are lower with the

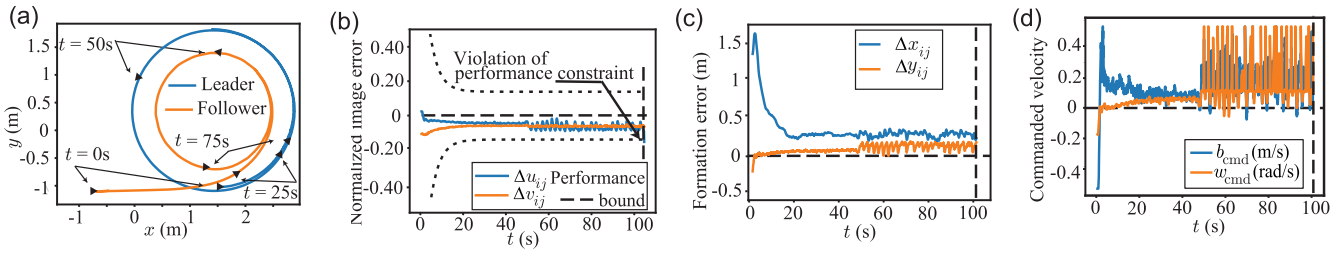

FIGURE 15. Experimental results obtained with the comparison controller in [1] for the varying velocity case. (a) Leader and follower trajectories with snapshots provided every 25 seconds. (b) Time-trajectories of normalized image-plane formation errors with vertical dashed line denoting the instant of loss of feature tracking and formation control due to violation of performance constraint. (c) Time-trajectories of formation errors in configuration space. (d) Control commands executed by the follower robot.

TABLE 1. Comparison of the root mean square error (RMSE) and mean absolute percentage error (MAPE) for various control schemes considered in this study.

Case	Metric	Proposed (9)		Proposed (21)		PTPB	Adaptive PI	Barrier function	PPC
		($\mu = 1$)	($\mu = 0.75$)	($\mu = 1$)	($\mu = 0.75$)	[13]	[31]	[12]	[1]
Constant leader velocity Input Effort	RMSE (mm)	**13.13**	15.80	17.08	21.11	162.04	17.29	86.6	224.23
	MAPE (%)	**0.65**	0.82	1.10	1.48	11.68	0.93	4.6	21.07
	$\|\|b_{cmd}\|\|$ (m/s)	1.765	1.790	1.787	1.782	1.755	1.739	1.796	**1.611**
	$\|\|w_{cmd}\|\|$ (rad/s)	**1.360**	1.374	1.398	1.379	1.388	1.431	1.461	1.435
Varying leader velocity Input Effort	RMSE (mm)	**13.00**	16.82	22.21	20.16	257.04	–	–	–
	MAPE (%)	**0.69**	0.78	1.11	1.20	19.79	–	–	–
	$\|\|b_{cmd}\|\|$ (m/s)	4.482	4.476	4.557	4.469	**4.460**	–	–	–
	$\|\|w_{cmd}\|\|$ (rad/s)	**3.225**	3.253	3.496	3.395	3.320	–	–	–

conventional PI sliding mode compared to the terminal non-singular sliding mode. Importantly, it is also apparent that the steady-state performance of either of the proposed schemes - (9) and (21) - is significantly superior to the rest of the control schemes chosen for comparison with similar levels of control effort. This can be attributed to the fact that the state-dependent structure of the perturbation term $\boldsymbol{g}(\boldsymbol{\zeta})\tilde{\boldsymbol{\alpha}}(\boldsymbol{\zeta}, t)$ is explicitly accounted for in the proposed designs of (9) and (21), which is not the case with the alternative designs in [12] and [13], while the adaptive PI strategy in [31] and the PPC strategy in [1] - which rely on performance constraints to regulate formation control with gain parameters tuned for the nominal case of constant leader velocity - fail in the presence of a varying leader velocity profile due to an abrupt and large increase in the magnitude of the disturbance term $\overline{\alpha}$ arising from a large increase in leader velocity. The video of the formation control experiments undertaken with the proposed schemes (9) and (21) can be found here.

VI. CONCLUSION

Two adaptive integral sliding mode control strategies are presented to solve the problem of finite-time convergence of a constrained and perturbed FOSM in this study. In particular, the main contribution lies in the synthesis of novel sliding-mode control schemes that rely on reduced *apriori* knowledge of the system uncertainty to achieve finite time convergence from any initial condition within the predefined state constraint set. This is accomplished by relying on a nonlinear map that transforms the constrained system into an unconstrained one, which subsequently enables the synthesis of adaptive integral control policies that guarantee finite-time convergence to a small bound using continuous and bounded control action. Experimental studies of leader-follower formation control are used to validate the performance of the proposed schemes in the presence of measurement noise. A detailed performance comparison study with leading alternative designs is also undertaken to demonstrate the superior performance of the proposed schemes. Future work would potentially expand this framework to accomplish higher order sliding mode control in the presence of constrained inputs.

REFERENCES

[1] J. Lin, Z. Miao, H. Zhong, W. Peng, Y. Wang, and R. Fierro, "Adaptive image-based leader-follower formation control of mobile robots with visibility constraints," *IEEE Trans. Ind. Electron.*, vol. 68, no. 7, pp. 6010–6019, Jul. 2021.

[2] I. Boiko, *Discontinuous Control Systems: Frequency Domain Analysis and Design*. Berlin, Germany: Springer, 2008.

[3] S. Roy, S. Baldi, and L. M. Fridman, "On adaptive sliding mode control without a priori bounded uncertainty," *Automatica*, vol. 111, Jan. 2020, Art. no. 108650.

[4] D. Y. Negrete-Chavez and J. A. Moreno, "Second-order sliding mode output feedback controller with adaptation," *Int. J. Adapt. Control Signal Process.*, vol. 30, nos. 8–10, pp. 1523–1543, 2016.

[5] Y. Chang, "Adaptive sliding mode control of multi-input nonlinear systems with perturbations to achieve asymptotical stability," *IEEE Trans. Autom. Control*, vol. 54, no. 12, pp. 2863–2869, Dec. 2009.

[6] T. R. Oliveira, J. P. V. S. Cunha, and L. Hsu, "Adaptive sliding mode control for disturbances with unknown bounds," in *Proc. 14th Int. Workshop Variable Struct. Syst. (VSS)*, Jun. 2016, pp. 59–64.

[7] B. Tian, J. Cui, H. Lu, Z. Zuo, and Q. Zong, "Adaptive finite-time attitude tracking of quadrotors with experiments and comparisons," *IEEE Trans. Ind. Electron.*, vol. 66, no. 12, pp. 9428–9438, Dec. 2019.

[8] Y. Shtessel, M. Taleb, and F. Plestan, "A novel adaptive-gain supertwisting sliding mode controller: Methodology and application," *Automatica*, vol. 48, no. 5, pp. 759–769, 2012.

[9] C. Edwards and Y. Shtessel, "Adaptive dual-layer super-twisting control and observation," *Int. J. Control*, vol. 89, no. 9, pp. 1759–1766, Sep. 2016.

[10] Y. B. Shtessel, J. A. Moreno, and L. M. Fridman, "Twisting sliding mode control with adaptation: Lyapunov design, methodology and application," *Automatica*, vol. 75, pp. 229–235, Jan. 2017.

[11] H. Obeid, S. Laghrouche, L. Fridman, Y. Chitour, and M. Harmouche, "Barrier function-based adaptive super-twisting controller," *IEEE Trans. Autom. Control*, vol. 65, no. 11, pp. 4928–4933, Nov. 2020.

[12] H. Obeid, L. M. Fridman, S. Laghrouche, and M. Harmouche, "Barrier function-based adaptive sliding mode control," *Automatica*, vol. 93, pp. 540–544, Jul. 2018.

[13] H. Ma, W. Liu, Z. Xiong, Y. Li, Z. Liu, and Y. Sun, "Predefined-time barrier function adaptive sliding-mode control and its application to piezoelectric actuators," *IEEE Trans. Ind. Informat.*, vol. 18, no. 12, pp. 8682–8691, Dec. 2022, doi: 10.1109/TII.2022.3143606.

[14] F. Plestan, Y. Shtessel, V. Brégeault, and A. Poznyak, "New methodologies for adaptive sliding mode control," *Int. J. Control*, vol. 83, no. 9, pp. 1907–1919, Sep. 2010.

[15] C. Edwards and Y. B. Shtessel, "Adaptive continuous higher order sliding mode control," *Automatica*, vol. 65, pp. 183–190, Mar. 2016.

[16] H. Yao, F. Gao, J. Huang, and Y. Wu, "Barrier Lyapunov functions-based fixed-time stabilization of nonholonomic systems with unmatched uncertainties and time-varying output constraints," *Nonlinear Dyn.*, vol. 99, no. 4, pp. 2835–2849, Mar. 2020.

[17] K. Mei and S. Ding, "Output-feedback finite-time stabilization of a class of constrained planar systems," *Appl. Math. Comput.*, vol. 412, Jan. 2022, Art. no. 126573.

[18] C.-C. Chen and Z.-Y. Sun, "A unified approach to finite-time stabilization of high-order nonlinear systems with an asymmetric output constraint," *Automatica*, vol. 111, Jan. 2020, Art. no. 108581.

[19] C. Chen, "A unified approach to finite-time stabilization of high-order nonlinear systems with and without an output constraint," *Int. J. Robust Nonlinear Control*, vol. 29, no. 2, pp. 393–407, Jan. 2019.

[20] W. Sun, S.-F. Su, Y. Wu, J. Xia, and V.-T. Nguyen, "Adaptive fuzzy control with high-order barrier Lyapunov functions for high-order uncertain nonlinear systems with full-state constraints," *IEEE Trans. Cybern.*, vol. 50, no. 8, pp. 3424–3432, Aug. 2020.

[21] W. Sun, S.-F. Su, G. Dong, and W. Bai, "Reduced adaptive fuzzy tracking control for high-order stochastic nonstrict feedback nonlinear system with full-state constraints," *IEEE Trans. Syst., Man, Cybern., Syst.*, vol. 51, no. 3, pp. 1496–1506, Mar. 2021.

[22] Z. Guo, T. R. Oliveira, J. Guo, and Z. Wang, "Performance-guaranteed adaptive asymptotic tracking for nonlinear systems with unknown sign-switching control direction," *IEEE Trans. Autom. Control*, vol. 68, no. 2, pp. 1077–1084, Feb. 2023.

[23] V. H. P. Rodrigues, L. Hsu, T. R. Oliveira, and L. Fridman, "Adaptive sliding mode control with guaranteed performance based on monitoring and barrier functions," *Int. J. Adapt. Control Signal Process.*, vol. 36, no. 6, pp. 1252–1271, Jun. 2022.

[24] L. Hsu, T. R. Oliveira, J. P. V. S. Cunha, and L. Yan, "Adaptive unit vector control of multivariable systems using monitoring functions," *Int. J. Robust Nonlinear Control*, vol. 29, no. 3, pp. 583–600, Feb. 2019.

[25] S. Ding, J. H. Park, and C.-C. Chen, "Second-order sliding mode controller design with output constraint," *Automatica*, vol. 112, Feb. 2020, Art. no. 108704.

[26] S. Ding, K. Mei, and S. Li, "A new second-order sliding mode and its application to nonlinear constrained systems," *IEEE Trans. Autom. Control*, vol. 64, no. 6, pp. 2545–2552, Jun. 2019.

[27] M. Rubagotti and A. Ferrara, "Second order sliding mode control of a perturbed double integrator with state constraints," in *Proc. Amer. Control Conf.*, Jul. 2010, pp. 985–990.

[28] G. P. Incremona, M. Rubagotti, and A. Ferrara, "Sliding mode control of constrained nonlinear systems," *IEEE Trans. Autom. Control*, vol. 62, no. 6, pp. 2965–2972, Jun. 2017.

[29] M. Spiller and D. Söffker, "Output constrained sliding mode control: A variable gain approach," *IFAC-PapersOnLine*, vol. 53, no. 2, pp. 6201–6206, 2020.

[30] P. Li, D. Liu, and S. Baldi, "Adaptive integral sliding mode control in the presence of state-dependent uncertainty," *IEEE/ASME Trans. Mechatronics*, vol. 27, no. 5, pp. 3885–3895, Oct. 2022, doi: 10.1109/TMECH.2022.3145910.

[31] Y. Song, Y. Wang, and C. Wen, "Adaptive fault-tolerant PI tracking control with guaranteed transient and steady-state performance," *IEEE Trans. Autom. Control*, vol. 62, no. 1, pp. 481–487, Jan. 2017.

[32] H. K. Khalil, *Nonlinear Systems*. Hoboken, NJ, USA: Prentice-Hall, 2002.

[33] X. Yu, Y. Feng, and Z. Man, "Terminal sliding mode control—An overview," *IEEE Open J. Ind. Electron. Soc.*, vol. 2, pp. 36–52, 2021, doi: 10.1109/OJIES.2020.3040412.

[34] C.-S. Chiu, "Derivative and integral terminal sliding mode control for a class of MIMO nonlinear systems," *Automatica*, vol. 48, no. 2, pp. 316–326, Feb. 2012.

[35] B. Ning, Q.-L. Han, and Z. Zuo, "Practical fixed-time consensus for integrator-type multi-agent systems: A time base generator approach," *Automatica*, vol. 105, pp. 406–414, Jul. 2019.

[36] E. Ivanjko, T. Petrinic, and I. Petrovic, "Modelling of mobile robot dynamics," in *Proc. 7th EUROSIM Congr. Model. Simul.*, vol. 2, 2010, pp. 1–9.

[37] S. Garrido-Jurado, R. Muñoz-Salinas, F. J. Madrid-Cuevas, and M. J. Marín-Jiménez, "Automatic generation and detection of highly reliable fiducial markers under occlusion," *Pattern Recognit.*, vol. 47, no. 6, pp. 2280–2292, Jun. 2014.

JISHNU KESHAVAN (Member, IEEE) received the B.Tech. degree in aerospace engineering from the Indian Institute of Technology Bombay, in 2004, and the M.S. and Ph.D. degrees in aerospace engineering from the University of Maryland, College Park, in 2007 and 2012, respectively. He is an Assistant Professor of mechanical engineering with the Indian Institute of Science, Bengaluru. His research interests are broadly in the areas of dynamical systems theory, data-driven nonlinear dynamics and control, and autonomous vision.

SAURABH BELGAONKAR received the B.Tech. degree in mechanical engineering from the National Institute of Technology, Warangal. He is currently pursuing the M.Tech. degree with the Indian Institute of Science, Bengaluru. His research interests are broadly in the areas of dynamics and control and autonomous vision.

SHREERAM MURALI received the B.E. degree in mechanical engineering from the Ramaiah Institute of Technology, Bengaluru, in 2021. He is currently a Project Associate with the Indian Institute of Science. His research interests are in the areas of vision-based control and motion planning for mobile robot navigation.